THE JOURNAL OF BIOLOGICAL CHEMISTRY VOL. 281, NO. 20, pp. 13979–13989, May 19, 2006

Protein-Membrane Interaction and Fatty Acid Transfer from Intestinal Fatty Acid-binding Protein to Membranes

*SUPPORT FOR A MULTISTEP PROCESS**

Received for publication, November 4, 2005, and in revised form, March 20, 2006 Published, JBC Papers in Press, March 21, 2006, DOI 10.1074/jbc.M511943200

Lisandro J. Falomir-Lockhart[‡1], Lisandro Laborde[‡], Peter C. Kahn[§], Judith Storch[¶2], and Betina Córsico[‡3]

From the [‡]Instituto de Investigaciones Bioquímicas de La Plata (INIBIOLP), CONICET-UNLP, Facultad de Ciencias Médicas, Calles 60 y 120, 1900-La Plata, Argentina and the Departments of [¶]Nutritional Sciences and [§]Biochemistry and Microbiology, Rutgers, State University of New Jersey, New Brunswick, New Jersey 08901-8525

Fatty acid transfer from intestinal fatty acid-binding protein (IFABP) to phospholipid membranes occurs during protein-membrane collisions. Electrostatic interactions involving the α-helical "portal" region of the protein have been shown to be of great importance. In the present study, the role of specific lysine residues in the α-helical region of IFABP was directly examined. A series of point mutants in rat IFABP was engineered in which the lysine positive charges in this domain were eliminated or reversed. Using a fluorescence resonance energy transfer assay, we analyzed the rates and mechanism of fatty acid transfer from wild type and mutant proteins to acceptor membranes. Most of the α-helical domain mutants showed slower absolute fatty acid transfer rates to zwitterionic membranes, with substitution of one of the lysines of the α_2 helix, Lys[27], resulting in a particularly dramatic decrease in the fatty acid transfer rate. Sensitivity to negatively charged phospholipid membranes was also reduced, with charge reversal mutants in the α_2 helix the most affected. The results support the hypothesis that the portal region undergoes a conformational change during protein-membrane interaction, which leads to release of the bound fatty acid to the membrane and that the α_2 segment is of particular importance in the establishment of charge-charge interactions between IFABP and membranes. Cross-linking experiments with a phospholipid-photoactivable reagent underscored the importance of charge-charge interactions, showing that the physical interaction between wild-type intestinal fatty acid-binding protein and phospholipid membranes is enhanced by electrostatic interactions. Protein-membrane interactions were also found to be enhanced by the presence of ligand, suggesting different collisional complex structures for holo- and apo-IFABP.

Intestinal fatty acid-binding protein (IFABP)[4] belongs to a family of intracellular lipid binding proteins of low molecular mass (14–15 kDa) with the putative general function of lipid trafficking (1). The precise physiological functions of these proteins are as yet unclear, but it is hypothesized that they are important in intracellular transport and targeting of FA to specific membranous organelles and metabolic pathways. Intestinal fatty acid-binding protein is abundantly produced in the enterocyte, where a second fatty acid-binding protein (FABP), liver FABP (LFABP), is also highly expressed (2). It is not known why a single cell type contains two distinct types of FABP nor whether one or both participate in the intracellular trafficking and compartmentation of lipid. A number of differences between the two enterocyte FABPs, in binding specificity and stoichiometry and in ligand transport properties, suggest unique functional properties (1, 3, 4). To address the putative transport function of the FABPs, we have used an *in vitro* fluorescence resonance energy transfer assay to examine the rate and mechanism of transfer of fluorescently tagged fatty acids from FABPs to phospholipid membranes. These studies have demonstrated that transfer of fatty acids from IFABP to membranes appears to occur during direct collisional interactions between the protein and the acceptor membrane (3). In contrast, LFABP employs a different FA transfer mechanism, involving an initial release of the ligand to the aqueous milieu prior to its membrane association (5). As discussed previously (3, 6), we hypothesize that "collisional" fatty acid transfer by IFABP may be necessary for specific targeting of this physiologically important lipid. Moreover, it is also possible that IFABP forms charge-charge interactions with acidic domains on membrane proteins, thereby facilitating the targeted transport of intracellular fatty acids. In addition, the absolute rate of fatty acid transfer by IFABP-membrane interaction is dramatically increased relative to off-rates for fatty acids from FABPs into solution, supporting the idea of greater efficiency of fatty acid trafficking via the collisional mechanism.

Fatty acid-binding proteins share a common tertiary structure consisting of 10 antiparallel β-strands that form a β-barrel, which is capped by two short α-helices arranged as a helix-turn-helix segment. It is believed that this helical domain is part of a "dynamic portal" that regulates fatty acid (FA) entry and exit from the internal binding cavity (7, 8). The structural elements underlying collisional transfer of a fatty acid from IFABP to membranes could have important physiological consequences, since they may dictate the fatty acid trafficking patterns within the cell. Using a helixless variant of IFABP (9) and employing chimeric proteins generated by exchanging the helix-turn-helix domains between IFABP and LFABP, we have demonstrated that the α-helical region of IFABP plays a primary role in the collisional transfer of fatty acid from IFABP to membranes (8, 10) and that this domain determines the unique FA transfer mechanism from LFABP or IFABP

* This work was supported by National Institutes of Health Grant DK 38389 (to J. S.) and Grant TW01100-01 (to J. S. and B. C.) and Fundación Antorchas Grant 14116-224 (to B. C.). The costs of publication of this article were defrayed in part by the payment of page charges. This article must therefore be hereby marked "*advertisement*" in accordance with 18 U.S.C. Section 1734 solely to indicate this fact.

[1] Recipient of a Doctoral Fellowship from the National Research Council (Consejo Nacional de Investigaciones Científicas y Técnicas) of Argentina.

[2] To whom correspondence may be addressed. Tel.: 732-932-1689; Fax: 732-932-6837; E-mail: storch@aesop.rutgers.edu.

[3] To whom correspondence may be addressed. Tel.: 54-221-482-4894; Fax: 54-221-425-8988; E-mail: bcorsico@atlas.med.unlp.edu.ar.

[4] The abbreviations used are: IFABP, intestinal fatty acid-binding protein; FA, fatty acids; FABP, fatty acid-binding protein; LFABP, liver fatty acid binding protein; wtIFABP, wild-type intestinal fatty acid binding protein; SUV, small unilamellar vesicle; LUV, large unilamellar vesicle; AOFA, anthroyloxy-labeled fatty acid; 12AO, 12-(9-anthroyloxy)oleic acid, EPC, egg phosphatidylcholine; PS, brain phosphatidylserine; CL, bovine heart cardiolipin; NBD-PC, *N*-(7-nitro-2,1,3-benzoxadiazol-4-yl) egg phosphatidylcholine; ^{125}I-TID-PC, 1-*O*-hexadecanoyl-2-*O*-[9-[[[2-[^{125}I]iodo-4-(trifluoromethyl-(3*H*)-diazirin-3-yl)benzyl]oxy]carbonyl]nonanoyl]-*sn*-glycero-3-phosphocholine; FA, fatty acid; ADIFAB, acrylodated IFABP; 12AO, 12-(9-anthroyloxy)oleic acid).

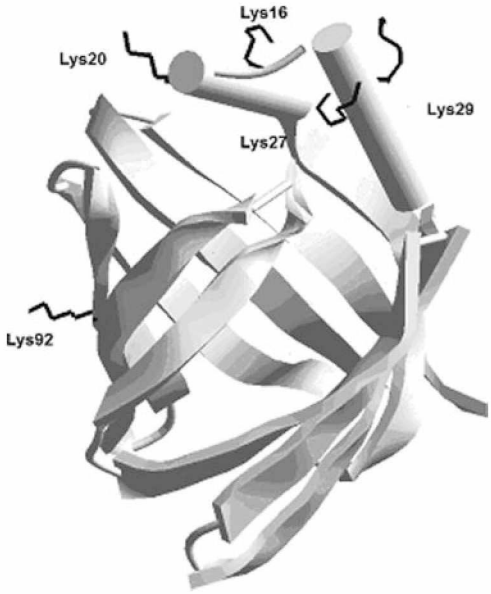

FIGURE 1. ***Ribbon diagram* of rat intestinal FABP derived from 2.0 Å resolution x-ray crystallography (20) (Protein Data Bank code 2IFB).** Lys^{16}, Lys^{20}, Lys^{27}, Lys^{29}, and Lys^{92} have been *highlighted* in a *stick representation*. The protein molecule is oriented to show the positions of mutated residues.

to acceptor membranes (4).[5] Abundant experimental evidence has indicated that electrostatic interactions are a major determinant of the mechanism of FA transfer from all of the "collisional" proteins of this family (adipocyte, heart, brain, myelin, and intestinal FABPs) (11–16). In addition, an analysis of surface electrostatic potential topologies for several FABPs demonstrated a net positive potential across the helix-turn-helix portal region of "collisional transfer" FABPs (17), which supports the suggestion that this region is important for interactions with membranes. It is noteworthy that the α_1 helices of IFABP, heart FABP, and adipocyte FABP are amphipathic, whereas α_1 helices of LFABP, liver basic FABP, and cellular retinoid-binding protein II, which do not employ a collisional ligand transfer mechanism, are not (18). Amphipathic helices are known to be important motifs in the targeting of proteins to membranes, and the charge characteristics of a helix are believed to modulate interactions with membranes (19).

In the present study, we tested the hypothesis that the lysine residues of the α-helical domain of IFABP play an important role in the collision-based transfer of FA to membranes. Several pairs of point mutants of IFABP were engineered so as to neutralize or reverse the positive charge of the lysines present in the α-helical domain (Lys^{16}, Lys^{20}, Lys^{27}, and Lys^{29}) as well as Lys^{92} in the β-barrel (Fig. 1). The primary objectives of this work were to determine whether the elimination of positively charged residues in the α-helical domain of IFABP would alter the rate and, potentially, the mechanism of transfer of FA from the mutant proteins to membranes, compared with the wild-type IFABP (wtIFABP), and to assess the relative contributions of each of the charged residues.

A fluorescence resonance energy transfer assay was used to assess the kinetics of FA transfer from FABPs to membranes, and direct interaction of the IFABPs with phospholipid membranes was determined using a cross-linking assay with vesicles containing a photoactivable reagent. The results demonstrate that no single lysine was solely responsible for the FA transfer properties of IFABP. Rather, all of the Lys residues of the α-helical domain contribute to the collisional mechanism of FA transfer from IFABP to model membranes. Lys residues of the α_2 segment are of particular importance in the FA transfer process.

[5] G. R. Franchini, B. Córsico, and J. Storch, unpublished observations.

EXPERIMENTAL PROCEDURES

Materials

The mutagenic primers were obtained from Invitrogen (Carlsbad, CA). *Pfu* DNA polymerase, pGEM-T easy vector, and restriction enzymes XbaI and BamHI were purchased from Promega (Madison, WI). T4 DNA ligase, pET-11a expression vector, and BL21 (DE3) cells were obtained from Novagen (Milwaukee, WI). Sodium oleate was obtained from Nu-Chek Prep (Elysan, MN). Fluorescently labeled AOFA, 12-(9-anthroyloxy)oleic acid (12AO), and acrylodated IFABP (ADIFAB) were purchased from Molecular Probes, Inc. (Eugene, OR). Egg phosphatidylcholine (EPC), *N*-(7-nitro-2,1,3-benzoxadiazol-4-yl) egg phosphatidylcholine (NBD-PC), brain phosphatidylserine (PS), and bovine heart cardiolipin (CL) were obtained from Avanti Polar Lipids (Alabaster, AL). Lipidex-1000 was purchased from Sigma. Isopropyl-β-D-thiogalactoside was obtained from Fisher. [^{125}I]NaI was from PerkinElmer Life Sciences. All other chemicals were reagent grade or better.

Construction of Point Mutant IFABPs

IFABP has four lysine residues in the helix-turn-helix domain, two in each α-helical segment. A series of point mutants were constructed substituting lysine for isoleucine to eliminate the charge and lysine for glutamic acid to reverse the charge. Isoleucine and glutamic acid were chosen to replace lysine due to their respective neutral and negative charges and the relatively similar bulkiness to lysine, so as to maintain the approximate side chain size along the backbone of the protein. Thus, eight mutations in the α-helical region were constructed, and an additional pair of mutants, K92I and K92E, was also generated to assess the effects of a nonhelix domain basic residue; Lys^{92} is located in β strand G. Recombinant rat pET11d-IFABP plasmid was generously provided by Drs. Alan Kleinfeld and Ron Ogata (Medical Biology Institute, La Jolla, CA). A single or double mutation was introduced in the IFABP sequence employing overlapping PCR methodology (20). The same external primers were used for all constructs: 5′-CGGATAACAATTCCCCTCTA-3′ and 5′-TTCCTTTCGGGCTTTGTTAG-3′. Each mutation was verified by sequence analysis. Mutant DNA sequences were subcloned into the pET-11a expression vector by using XbaI and BamHI restriction sites.

Protein Expression and Purification

All proteins were overexpressed in *Escherichia coli* BL21 DE3 harboring pET constructs for wild-type and point mutant proteins, as detailed elsewhere (3, 8); all of the proteins were found in the soluble fraction of the bacterial lysates and were purified from *E. coli* as described previously (3, 8).

Analysis of Wild-type and Mutant FABPs

None of the lysine residues mutated in this study are found within the ligand binding site (21); thus, maintenance of binding site integrity was expected. To assess this directly, the overall conformation and ligand binding site properties of the mutant IFABPs were examined by several methods.

Molecular Modeling—Crystallographic structures of rat apo-IFABP (Protein Data Bank code 1IFC) (21) and rat holo-IFABP with palmitate bound (Protein Data Bank code 2IFB) (22), solved at 2.0 and 1.2 Å, respectively, were used to model the mutant proteins. Silicon Graphics workstations running the InsightII program (Accelrys, San Diego, CA) were used to replace amino acids to generate initial models, one single

site replacement for each mutant protein. We then performed conformational energy minimization, first adding hydrogens to the structures, since the Protein Data Bank files contained heavy atoms only. The modeling pH was set to 7.4. The "soak" facility of InsightII was used to create a layer of water molecules around the protein 5.0 Å thick. Water molecules present in the crystallographic files were retained prior to "soaking" as well as the bound palmitate in the holo structure. The energy was then minimized to convergence using default settings. The wild type molecules in the PDB files were also minimized in order that comparisons between wild type and mutants would compare structures that had been treated identically. Bond lengths, bond angles, and Ramachandran plots were normal (data not shown). Analysis of solvent-accessible surface area was by the method of Lee and Richards (23) using the program ACCESS (24). The ACCESS output was sorted and compiled by BINS (25), which classifies each atom as to whether it is aliphatic, aromatic, polar uncharged, or polar charged and aggregates the results for each amino acid and for the protein as a whole. Volumes were computed by the Voronoi method with the program VOLUME, the output being compiled by VOLFMT (26, 27).

CD Spectra—CD spectra were obtained at 25 °C on an Aviv model 60DS spectropolarimeter using a 0.1-cm path length quartz cuvette (Hellma). Spectra of the wild-type and mutant proteins were obtained from five scans between 200 and 260 nm of a 0.15 mg/ml protein concentration solution to evaluate shape, ellipticity, and maximum and minimum positions.

Fluorescent Quantum Yields—Fluorescent quantum yields (Q_f) of 12-(9-anthroyloxy)oleic acid (12AO) bound to wild-type and mutant IFABPs were determined using quinine sulfate in 0.1 N H_2SO_4 as the reference fluorophore, with $Q_{ref} = 0.7$ (28). Excitation was at 352 nm for quinine sulfate and 383 nm for 12AO.

Binding of Oleate—Binding of oleate to wild-type and mutant IFABPs was analyzed by the method employing the fluorescent probe ADIFAB (29), which allows for the direct measurement of unbound fatty acid in equilibrium with FABP. Oleate prepared as a 25 mM stock solution of the sodium salt in water at pH 9.7 containing 25 μM BHT was titrated into 2.5 ml of 10 mM HEPES, 150 mM NaCl, 5 mM KCl, and 1 mM Na_2HPO_4 (pH 7.4) containing 0.2 μM ADIFAB and 4 μM wild type or mutant IFABP. Following equilibration at 37 °C for 5 min, fluorescence emission intensities at 505 and 432 nm were measured using an SLM-8000C spectrofluorometer, with excitation at 386 nm. The average and S.D. of 10 pairs of R (emission 505 nm/emission 432 nm) values were determined. This average was applied to binding equilibrium analysis using a standard value of $R_{max} = 11.5$ (29). Experimental values were fitted to a single-site Scatchard analysis, and K_d values for oleate binding were obtained.

Relative Partition Coefficient—The relative partition coefficient (Kp) for AOFA partitioning between wild type or mutant IFABPs and small unilamellar vesicles (SUVs) was determined by measuring AOFA fluorescence at a given molar ratio of protein/SUV after titration of SUV into a solution containing 5 μM protein and 0.5 μM 12AO in 40 mM Tris, 100 mM NaCl, pH 7.4 (TBS) at 25 °C (30, 31).

$$K_p = \frac{([\text{FABP-bound AOFA}]/[\text{FABP}])}{([\text{SUV-bound AOFA}]/[\text{SUV}])} \quad \text{(Eq. 1)}$$

The decrease in AOFA fluorescence upon titration of AOFA-containing FABP with SUVs was related to Kp by the following equation,

$$1/\Delta F = 1/K_p(1/\Delta F_{max})([\text{FABP}]/[\text{SUV}]) + 1/\Delta F_{max} \quad \text{(Eq. 2)}$$

where ΔF is the difference between the initial fluorescence of AOFA in the FABP and the AOFA fluorescence at a given protein/SUV ratio, and ΔF_{max} is the maximum difference in AOFA fluorescence. A plot of $1/\Delta F$ *versus* $(1/\Delta F_{max})([\text{SUV}]/[\text{FABP}])$ gives a slope of $1/Kp$. The partition coefficient was used to establish AOFA transfer assay conditions so as to ensure essentially unidirectional transfer, as detailed below (32).

Vesicle Preparation for AOFA Transfer Experiment

SUVs were prepared by sonication and ultracentrifugation as described previously (33, 34). The standard vesicles were prepared to contain 90 mol % of EPC and 10 mol % of NBD-PC, which served as the fluorescent quencher. To increase the negative charge density of the acceptor vesicles, either 25 mol % of PS or CL were incorporated into the SUVs in place of an equimolar amount of EPC. Vesicles were prepared in TBS buffer except for SUVs containing cardiolipin, which were prepared in TBS with 1 mM EDTA.

Transfer of AOFA from FABP to SUV

A fluorescence resonance energy transfer assay was used to monitor the transfer of AOFA from the wild type and mutant IFABPs to acceptor model membranes as described in detail elsewhere (3, 4, 8). Briefly, FABP with bound AOFA was mixed at 25 °C with SUV using a stopped-flow spectrofluorometer DX-17MV (Applied Photophysics Ltd.). The NBD moiety is an energy transfer acceptor of the anthroyloxy group donor; therefore, the fluorescence of the AOFA is quenched when the ligand is bound to SUVs that contain NBD-PC. Upon mixing, transfer of AOFA from protein to membrane is directly monitored by the time-dependent decrease in anthroyloxy group fluorescence. Final transfer assay conditions were 15 μM wild-type or mutant IFABP with 1.5 μM 12AO and a range of 150 – 600 μM SUV. Controls to ensure that photobleaching was eliminated were performed prior to each experiment, as previously described (8). Data were analyzed using software provided with the instrument, and all curves were well described by a single exponential function. For each experimental condition within a single experiment, at least five replicates were done. Average values ± S.D. for three or more separate experiments are reported, unless otherwise indicated.

Preparation of Photoactivable Reagents

^{125}I-TID-PC was prepared by radioiodination of its nonradioactive tin-containing precursor 1-*O*-hexadecanoyl-2-*O*-[9-[[[2-(tributylstannyl)-4-(trifluoromethyl-(3*H*)-diazirin-3-yl)benzyl]oxy]carbonyl]nonanoyl]-*sn*-glycero-3-phospho-choline according to Weber and Brunner (35) and our previous work (36). The precursor was generously donated by Prof. J. Brunner from the Swiss Federal Institute of Technology (Zurich, Switzerland). The dried tin-containing precursor (~20 nmol) was dissolved in 10 μl of acetic acid in a 1-ml Reacti-Vial (Pierce). [^{125}I]NaI (1 mCi) was added, and the iodination was started by the addition of peracetic acid (2 μl of a 32% solution in acetic acid). After 2 min at room temperature, the reaction was quenched with 50 μl of 10% $Na_2S_2O_5$. Then 40 μl of chloroform/methanol (2:1) were added and vortexed. The organic phase was collected and concentrated using a charcoal filter to adsorb volatile radioactivity. The residue was dissolved in 20 μl of methanol/chloroform/H_2O (9:1:1) and subjected to reverse-phase high pressure liquid chromatography using the same solvent and a 208HS54 C8 column (Vydac) in a Merck-Hitachi apparatus with UV detection at 254 nm. The flow rate was 1 ml/min, and fractions of 0.5 ml were collected. ^{125}I-TID-PC eluted at ~20 min, whereas the excess of tin-containing precursor eluted at ~40 min. An aliquot (5 μl) of each fraction in the elution region of ^{125}I-TID-PC was analyzed by TLC on silica gel plates (LK6D, 60 Å; Whatman, Clifton, NJ) and subjected to autoradiography.

TABLE 1

Energy minimization and physical and binding parameters of wild-type and mutant IFABPs

Conformational energy minimization was performed on wild type and mutant proteins (modeled from crystallographic structures) employing the Insight II program as described under "Experimental Procedures." Expressed wild type and mutant IFABP were analyzed for circular dichroism spectroscopic properties (θ_{222}), apparent ligand dissociation constants (K_d), coefficients for AOFA partitioning (Kp) between SUVs and FABPs, and fluorescent quantum yields (Q_f), as outlined under "Experimental Procedures." ND, not determined. Results for K_d, Kp, and Q_f are the average of three separate experiments ± S.D. except those indicated with an asterisk.

	Energy		θ_{222}	K_d	Kp	Q_f
	Apo	Holo				
	kcal/mol		*degrees* M^{-1} cm^{-1}	*nM*	*[SUV]/[prot]*	
wtIFABP	−15,304	−12,027	−5265	37 ± 1	12.5 ± 5.7	0.08 ± 0.02
K16I	−15,302	−11,934	−9026	45 ± 1	21.8 ± 5.9	0.08 ± 0.03
K16E	−15,418	−12,064	ND	32 ± 6	13*	0.08 ± 0.02
K20I	−15,227	−12,251	−7662	40 ± 7	18.5 ± 0.7	0.11 ± 0.04
K20E	−15,359	−12,012	−9883	41 ± 16	20*	0.11 ± 0.03
K27I	−15,333	−12,005	−9887	35 ± 3	11.8 ± 4.0	0.14 ± 0.04
K27E	−15,425	−12,035	ND	57 ± 2	14.7*	0.07 ± 0.02
K29I	−15,302	−12,017	−8683	28*	19.1*	0.15 ± 0.04
K29E	−15,429	−12,122	−4583	21*	14.5*	0.18 ± 0.05
K92I	−15,176	−11,934	−4994	49*	ND	0.12 ± 0.07
K92E	−15,209	−12,058	−5839	61*	9.5*	0.13 ± 0.07

Fractions containing radioactivity were pooled and concentrated by co-evaporation with toluene/ethanol (1:1). ^{125}I-TID-PC was dissolved in ethanol/toluene (1:1) at ~1 mCi/ml and stored at −20 °C.

Preparation of Lipid Vesicles Containing ^{125}I-TID-PC

Large unilamellar vesicles (LUVs) of EPC, EPC/PS (3:1, mol/mol), or EPC/CL (3:1, mol/mol) were prepared (0.5 mM in phospholipids) by extrusion through polycarbonate membranes of 100-nm pore diameter (Avestin Inc., Ottawa, Canada). To prepare the LUVs containing ^{125}I-TID-PC (200 μCi/μmol of phospholipids), the photoreagent was mixed with the lipids in chloroform. Lipids in chloroform were mixed, dried under a stream of N_2, and resuspended in 40 mM Tris, 100 mM NaCl, 50 mM glutathione (buffer A) by vortexing. Cardiolipin-containing vesicles also had 1 mM EDTA included in the buffer A. Then lipid suspensions were incubated at 37 °C for 30 min and passed 11 times through the polycarbonate filters using a Liposofast extruder system (Avestin).

Photolabeling Analysis of FABP-Membrane Interactions

Experiments were conducted as previously described (36). Briefly, 120 μl of 0.5 mM photoreagent-containing LUVs (30 μCi/ml) were incubated with the 60 μg of FABP in 200 μl of buffer A at room temperature for 30 s. In those experiments where oleate was included, we employed a 10:1 protein/ligand (mol/mol) ratio, and the protein-ligand complex was prepared prior to the incubation with LUVs. After the indicated incubation time, mixtures (0.3 ml) in glass cuvettes were irradiated for 30 s with a xenon lamp (450 watts) at a distance of 25 cm. As a control, the photoreagent-containing LUVs were irradiated prior to their mixture with IFABP. After irradiation, 3 volumes of $CHCl_3$/methanol (2:1) were added and vortexed, and the organic phase was discarded. FABPs were precipitated with 5 volumes of acetone and redissolved in 25 μl of sample buffer for direct analysis by SDS-PAGE (37). Following Coomassie Blue staining, gels were dried and exposed to X-Omat film (Eastman Kodak Co.) at −80 °C for different times, depending on the amount of radioactivity.

RESULTS

Construction of Mutant Proteins and Comparison of Structural and Ligand-binding Properties with Native IFABP—To examine whether the primary determinant of the IFABP fatty acid transfer mechanism resides in the lysine residues of the helix-turn-helix domain, we undertook the construction of point mutants that neutralized or reversed the charges of the four lysines of the α-helical domain and one of the lysine residues of the β-barrel. To control for potential alterations in the overall folding of the point mutants, molecular modeling, circular dichroism spectroscopy, fluorescence quantum yield measurements of bound anthroyloxy fatty acid, equilibrium binding affinity of oleate using the ADIFAB method, and determination of the relative partition coefficient of 12AO between the IFABPs and SUVs were used. A summary of the results for these experiments is presented in Table 1.

Conformational energy minimization calculations of the mutant IFABPs were performed for both apo and holo forms of the mutant proteins and compared with the wild-type protein, which was also subjected to energy minimization. As shown in Table 1, the differences in the overall conformational energy of the mutant proteins compared with the native IFABP were small, ranging from 0.01 to 1.87%. The solvent-accessible surface areas were found to be similar to that calculated for the native protein, and the mutant apo-IFABP forms also showed protein volume values similar to that of the wild-type apo-IFABP (Table 2). For the holoproteins, K27I was found to have a 0.42% increase in protein volume, whereas all other mutations resulted in somewhat lower volumes than the wild type. When the 95% confidence limit for the mean areas and volumes is calculated, it is seen that none of the individual mutant or wild type values fall outside the limits. This is consistent with the absence of significant conformational change due to the mutations.

To examine the likely conformation of the portal domain (residues 24–33, 54–55, and 73–74), the backbone of the rest of the protein (residues 2–22, 35–52, 57–71, and 76–130) was superimposed, and the result for the minimized holo structures showed that little change was introduced by the point mutations to the conformation of the protein. Table 3 shows the root mean square displacement for the protein's heavy atoms, grouped by structural regions. Not surprisingly, relatively larger effects were found in the portal regions for the α-helix mutants and in the β-barrel for the K92 mutations. As a comparison, superimposition of minimized apo- and holo-IFABPs showed ~3-fold greater root mean square displacement than any of the point mutants. Together, these estimations suggest that, as anticipated, the point mutations did not change the overall protein structure to a great extent.

A one-tailed t test comparing the root mean square displacements of the portal and nonportal regions of the protein was performed. Because the variance for the different groups of regions is not the same (F-test, $p < 0.01$), the t test for unequal variance was used. It shows that the portal region displacements exceed the nonportal displacements ($p < 0.02$).

The CD spectrum of the wild-type protein was found to agree in shape and intensity with previously published results (4, 38). The

TABLE 2

Solvent-accessible surface area and protein volume estimations of wild-type and mutant IFABPs

Solvent-accessible surface area (SAS) and protein volume (PV) were determined as described under "Experimental Procedures."

Protein	SAS		PV	
	Apo	Holo	Apo	Holo
	$Å^2$		$Å^3$	
Wild type	7033	7075	19,676	20,190
K16I	7030	7028	19,513	18,806
K16E	6986	7013	19,654	19,374
K20I	7066	7027	19,616	19,202
K20E	6979	7031	19,473	19,437
K27I	7046	7013	19,417	20,274
K27E	7125	7068	19,599	19,544
K29I	7016	7019	19,621	18,973
K29E	7160	7168	19,669	19,204
K92I	6984	6986	19,576	19,242
K92E	6994	6998	19,619	19,295
Mean $\pm$ $t_{½}$ $\times$ S.D.	7038 $\pm$ 156	7039 $\pm$ 132	19,585 $\pm$ 220	19,413 $\pm$ 1195

TABLE 3

Average displacement in the superimposition of minimized structures of mutant and wild-type IFABPs

Root mean square displacement (RMSD) in the superimposition of backbone of the nonportal regions of the minimized holo structures of mutant IFABP with the native protein.

Protein	RMSD		
	All heavy atoms (residues 1–131)	Nonportal regions (residues 2–22, 35–52, 57–71, 76–130)	Portal regions (residues 24–33, 54–55, 73–74)
		$Å$	
K16I	0.55	0.53	0.73
K16E	0.6	0.61	0.63
K20I	0.62	0.62	0.69
K20E	0.51	0.46	0.8
K27I	0.51	0.46	0.69
K27E	0.5	0.47	0.61
K29I	0.46	0.43	0.67
K29E	0.52	0.44	0.93
K92I	0.43	0.43	0.35
K92E	0.45	0.47	0.35
Mean $\pm$ $t_{½}$ $\times$ S.D.	0.52 $\pm$ 0.17	0.49 $\pm$ 0.19	0.65 $\pm$ 0.48
Apo- *versus* holo-WT	1.51	1.44	1.65

mutant IFABP spectra were similar to the wild type protein spectrum, with all showing a minimum at 215 nm (not shown). Values of the molar ellipticity at 222 nm, θ_{222}, for wtIFABP and the mutant IFABPs are shown in Table 1. It is likely that the variability in θ_{222} for some of the mutants is due to slight errors in protein concentrations of the solutions rather than conformational changes.

Fluorescence quantum yields (Q_f) for the AOFA are used to assess the relative hydrophobicity of the environment surrounding the fluorophore (12, 13, 28, 39). The comparison of 12AO Q_f values for the mutant and native proteins could therefore indicate whether the modifications introduced to the native protein may have altered the dielectric environment of its binding pocket. We found that the Q_f values for the mutant proteins were close to those obtained for the wtIFABP (Table 1), suggesting that the modification introduced in the α-helical domain did not modify the hydrophobicity of IFABP ligand binding site.

The fluorescent probe ADIFAB, an IFABP covalently modified with an acrylodan fluorophore, was used to assess the equilibrium binding affinity of the fatty acid oleate. Binding of FA to ADIFAB induces a red shift in the acrylodan emission spectrum, and this is used to provide a measure of unbound FA in solution (29). Using the known K_d of ADIFAB for a particular ligand (29), equilibrium binding affinities can be determined for another protein. The K_d obtained for oleate binding to wtIFABP (37 $\pm$ 1 nM) is in agreement with those previously determined (4, 29). Data for the mutants demonstrated a single binding site with K_d values similar to that obtained for the wild type protein (Table 1).

An apparent partition coefficient value was also obtained for each protein, describing the relative distribution of 12AO between an FABP and EPC-SUVs. This value was determined by adding SUVs containing the energy transfer quencher NBD-PC to a solution containing a preformed 12AO-FABP complex. With the successive addition of increasing amounts of the SUVs, a decrease in fluorescence emission was observed upon net displacement of fatty acid to the SUVs. Analysis of these data, as described under "Experimental Procedures," showed a preferential partitioning of 12AO to the SUVs (Table 1), in agreement with previous results (40). The partition coefficients for 12AO distribution between the mutant proteins and EPC SUVs are very similar to that for the wild-type protein. These results indicate that, as for the native ligand, oleate, the relative affinity of the mutant proteins for 12AO is essentially unchanged compared with the wild-type IFABP. The similar *Kp* values obtained indicated that in the AOFA transfer assays, the same protein/SUV ratios as those employed for the wild-type protein, could be employed.

Overall, the controls suggest no major alterations in the conformation and binding site properties of the mutant IFABPs relative to their parent wild-type protein. All mutants fold properly and bind a single FA molecule in a relatively hydrophobic binding site.

Effect of Vesicle Concentration on AOFA Transfer from FABPs to Membranes—The effect of acceptor membrane phospholipid concentration on rates of ligand transfer has been used to distinguish between an aqueous diffusion mechanism, where no effect is observed, and a collision-mediated mechanism, where the ligand transfer rate is directly related to the donor-acceptor collisional frequency and, hence, the vesicle concentration (3–5, 8). To distinguish between these transfer mechanisms, AOFA transfer from the mutant proteins to model zwitterionic

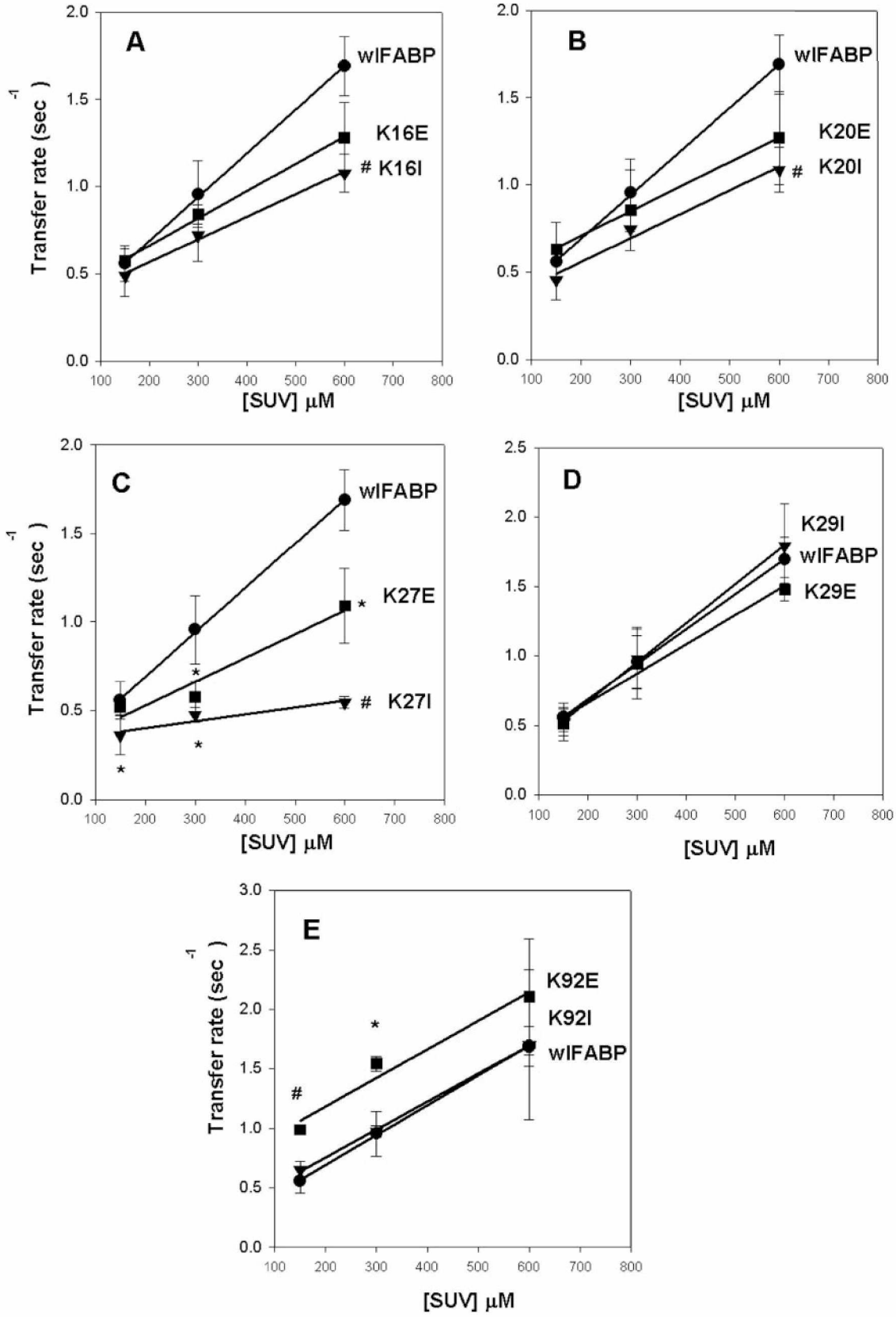

FIGURE 2. **Effect of acceptor membrane concentration on 12AO transfer from FABPs to zwitterionic SUVs.** Final concentrations were 15 μM FABP with 1.5 μM 12AO and 150 – 600 μM EPC-NBD acceptor vesicles. Each *panel* represents the results of the neutralization (▼) and reversion (■) mutants for a specific position, compared with the wild-type IFABP (*wI*) (●). *A*, K16I and K16E; *B*, K20I and K20E; *C*, K27I and K27E; *D*, K29I and K29E; *E*, K92I and K92E. The values shown are the mean ± S.D. from three sets of experiments. Two-tailed paired *t*-tests were used to determine the significant differences for each mutant *versus* wild-type IFABP for each concentration. $p < 0.05$ (*) and $p < 0.01$ (#) are presented.

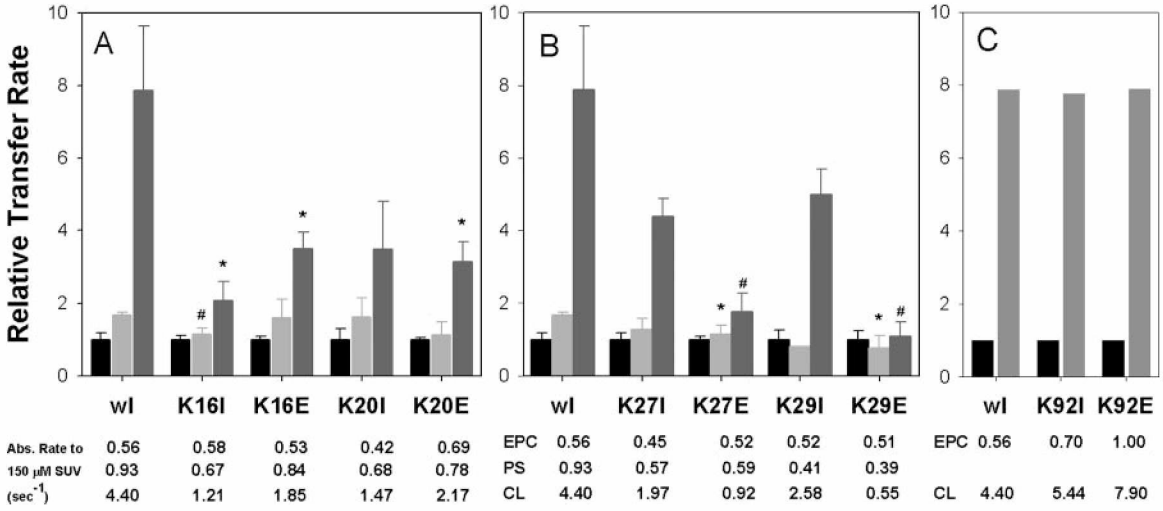

FIGURE 3. **Effect of vesicle charge on AOFA transfer from FABPs.** Transfer of 1.5 μM 12AO from 15 μM wtIFABP (*wI*) or mutant proteins to 150 μM EPC/NBD-PC SUV or 150 μM EPC/NBD-PC SUV containing 25 mol % of PS or CL. Results are expressed relative to the transfer rate of 12AO to EPC/NBD-PC SUV. SUVs of different composition are represented by *bars* in *black* (EPC/NBD-PC SUV), *light gray* (PS/NBD-PC SUV), and *dark gray* (CL/NBD-PC SUV). The values shown are the mean ± S.D. from three sets of experiments. *A*, transfer from α_1 mutants. *B*, transfer from α_2 mutants. Two-tailed paired *t*-tests were used to determine the significant differences for each mutant *versus* wtIFABP for each SUV composition. $p < 0.05$ (*) and $p < 0.01$ (#) are presented. *C*, transfer from β-barrel mutants. Transfer rates of 12AO to CL/NBD-PC SUV are expressed relative to the transfer rate of 12AO to EPC/NBD-PC SUV. The values shown in *C* correspond to a single experiment. The absolute rates of FA transfer from the various proteins to 150 μM EPC, PS, and CL-vesicles are listed, corresponding from *top* to *bottom* to EPC-, PS-, and CL-containing SUVs respectively.

membranes was examined as a function of increasing SUV concentration, and results were compared with those for the wild-type IFABP, a well characterized example of an FABP with a collisional ligand transfer mechanism. Fig. 2 shows the results obtained when constant concentrations of these FABP·AOFA donor complexes were mixed with increasing concentrations of EPC SUVs. Wild-type IFABP showed an almost proportional increase in transfer rates, ranging from 0.56 ± 0.10 to 1.69 ± 0.17 s^{-1}, to 150–600 μM SUV, similar to previous results (3, 8). All point mutants examined exhibit a nearly proportional increment in 12AO transfer rate as a function of vesicle concentration. This suggests that they all maintain the collisional mechanism of FA transfer characteristic of the wtIFABP. Nevertheless, the position of the lysine modification was important in determining the absolute AOFA transfer rates. Transfer rates from the α_1 helical mutants were lower than rates from the wild-type IFABP. For both Lys^{16} and Lys^{20}, a larger impact was observed when lysine was substituted with isoleucine (~36%) than the substitution for a glutamic acid (~25% decrease). Notably, the neutralizations (Lys → Ile mutants) in positions 16 and 20 produce exactly the same effects, and the same happens with the charge reversals (Lys → Glu mutants) in the same residues.

In contrast to the α_1 helical lysine mutants, the behavior of the two lysine residues of the α_2 helix was divergent. The largest impact of any of the point mutations was found for the K27I, exhibiting up to a 70% decrease in transfer rate to EPC SUV relative to wild type IFABP. In contrast, AOFA transfer rates from K29I and K29E mutants were little different from those of IFABP.

Nonportal neutralization mutant at position 92 did not show any difference compared with the wtIFABP. Surprisingly, reversion of the positive charge at the same position (K92E) results in a significant increase in AOFA transfer rates compared with those of wtIFABP (Fig. 2*E*).

Effect of Vesicle Charge on AOFA Transfer from FABPs to Membranes—Changes in the surface charge properties of the acceptor vesicles can also influence ligand transfer rates if electrostatic interactions between donor protein and acceptor membranes are involved, whereas in the case of aqueous diffusion, characteristics of the acceptor membrane would not be expected to modulate the transfer rate. Fig. 3 shows that, as expected from previous studies, the 12AO transfer rate from wtIFABP is substantially increased by incorporation of 25 mol % PS or CL into EPC/NBD-PC acceptor membranes (4, 8). A 2-fold increase for wtIFABP, on average, was observed in the absolute rate of 12AO transfer to PS-containing vesicles, from 0.56 ± 0.10 to 0.93 ± 0.05 s^{-1} for transfer to 150 μM EPC and PS acceptor SUVs, respectively. Incorporation of negatively charged CL in acceptor phospholipid vesicles resulted in a dramatic 8-fold increase in AOFA transfer rate from IFABP relative to transfer to zwitterionic vesicles.

Fig. 3*A* shows the relative transfer rates from wtIFABP and the α_1 helix mutants to EPC-containing, PS-containing, and CL-containing vesicles, normalized to the EPC acceptor for each protein. Overall, point mutants of lysine residues in the α_1 helix resulted in modest decreases in sensitivity to vesicle negative charge. Incorporation of CL into the acceptor vesicles resulted in approximately 3–4-fold increases in AOFA transfer rate relative to rates to EPC, as compared with the 8-fold stimulation observed for wtIFABP. K16I showed the greatest effect, with acceptor membrane CL causing only a 2-fold increase in AOFA transfer rate. For transfer to PS-containing membranes, only K16I showed a decrease in relative transfer rate.

Point mutations in the α_2 region showed a consistent pattern for neutralization *versus* charge reversal for both of the lysines. Neutralization did not induce significant decreases in AOFA transfer rate to either PS or CL vesicles, compared with wtIFABP (Fig. 3*B*). Moreover as for wtIFABP, both K27I and K29I showed a significant increase in 12AO transfer rate to CL vesicles relative to EPC vesicles. On the other hand, reversion mutants showed substantial decreases in AOFA transfer rates to PS vesicles and the most dramatic decreases in transfer rates to CL vesicles (78% ($p < 0.01$) for K27E, and 86% for K29E ($p < 0.01$)) compared with the wild-type protein (Fig. 3*B*). Indeed, charge reversal mutants K27E and K29E showed no significant modification of AOFA transfer rates to vesicles of different composition, as confirmed by analysis of variance ($p > 0.05$).

Neutralization of Lys^{92} to isoleucine or conversion to a negatively charged glutamate had little effect on the absolute rates of AOFA transfer to membranes or on the sensitivity to negative charge (Fig. 3*C*).

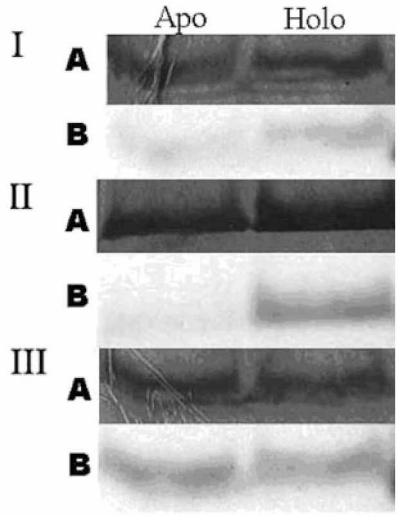

FIGURE 4. **Photolabeling of apo- and holo-IFABP by incubation with membranes of different composition containing ^{125}I-TID-PC.** Each *panel* corresponds to vesicles of different composition: EPC-^{125}I-TID-PC (*I*), PS-^{125}I-TID-PC (*II*), and CL-^{125}I-TID-PC (*III*). Experiments were conducted as indicated under "Experimental Procedures." Results of one representative experiment of three are presented. SDS-PAGE (*A*) and autoradiography (*B*) are shown in each *panel*. Quantification of the radioactive labeling in the autoradiography was performed using the ImageJ program (developed by the National Institutes of Health) as described under "Experimental Procedures." Values were expressed relative to the mass of the protein in the SDS-polyacrylamide gel, quantified with the same program, and normalized (1.0) to apo-wtIFABP incubated with EPC LUVs. Results were 1.34 ± 0.14 for holo-wtIFABP incubated with EPC LUVs. Incubation with acidic vesicles resulted in 1.03 ± 0.05 and 1.50 ± 0.08 (PS LUVs) and 1.38 ± 0.45 and 1.92 ± 0.37 (CL LUVs) for apo- and holo-wtIFABP, respectively. Averages of three separate experiments ± S.D. are shown.

Interaction of Intestinal FABP with Phospholipid Membranes—To analyze directly the interaction of FABPs with membranes, we conducted a series of experiments with membranes containing the photoactivable reagent ^{125}I-TID-PC. Upon photolysis, the trifluoromethyl diazirine group of this reagent is capable of reacting with protein segments inserted into or in contact with the hydrophobic region of the phospholipid membrane. These experiments were conducted to (*a*) determine the effect of the presence of ligand and the charge of the membrane on IFABP-membrane interaction and (*b*) detect specific domains and/or residues involved in the IFABP-membrane interaction. We examined apo- and holo- IFABP, as well as the helixless IFABP (9) and the point mutants K27E and K29E, for their interactions with zwitterionic and acidic phospholipid vesicles. Fig. 4 shows a representative result of three separate experiments, which suggests that the holo-IFABP interacts to a 30 and 50% greater extent than the apo-IFABP with 100% phosphatidylcholine vesicles and vesicles containing 25% PS, respectively. This difference between holo- and apoproteins almost disappears when IFABP is incubated with CL-containing vesicles, where both apo- and holo-IFABP interact strongly. The results in Fig. 4 also demonstrate an ~40% increase in the degree of interaction between IFABP and negatively charged vesicles compared with neutral vesicles.

To begin to assess the structural determinants of IFABP interaction with membranes, we selected mutants K27E and K29E due to their dramatic decrease in sensitivity to negatively charged vesicles in the FA transfer assay and examined their interaction with acidic membranes. The results in Fig. 5 show only small if any changes in apparent interactions, compared with the wild type protein (Fig. 5*I*). To examine the participation of the entire α-helical domain in the physical interaction with membranes, we used the helixless variant of IFABP, which lacks entirely the 17 residues of the α-helical domain (9). Helixless IFABP does not show appreciable labeling either with zwitterionic (not shown)

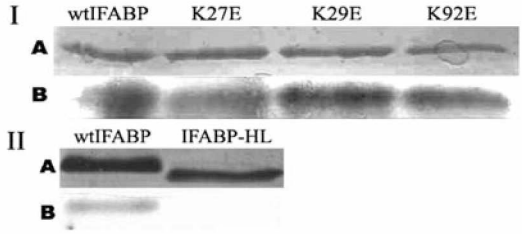

FIGURE 5. **Photolabeling of wild-type FABP, K27E, K29E, and K92E (*I*) and wtIFABP and helixless IFABP (*IFABP-HL*) (*II*) by incubation with acidic membranes containing ^{125}I-TID-PC and 25% CL.** Experiments were conducted as indicated under "Experimental Procedures." Results of one representative experiment of three are presented. SDS-PAGE (*A*) and autoradiography (*B*) are shown in each *panel*. Quantification of the radioactive labeling in the autoradiography was performed using the ImageJ program (developed by the National Institutes of Health) as described under "Experimental Procedures." Values are expressed relative to the mass of the protein in the SDS-polyacrylamide gel, quantified with the same program, and normalized (1.0) to wtIFABP incubated with CL-containing LUVs. Results were 0.82 ± 0.28 for K27E, 1.41 ± 0.61 for K29E, 1.33 ± 0.48 for K92E, and 0.10 ± 0.17 for helixless IFABP. Averages of three separate experiments ± S.D. are shown.

or acidic vesicles (Fig. 5*II*), suggesting that interaction of IFABP with membranes is diminished when the helical domain is absent.

DISCUSSION

In the present studies, we have examined the effects of eliminating or reversing the charge of the IFABP lysine residues in the α-helical domain in order to further understand the structural basis underlying the fatty acid transfer mechanism of IFABP. The mutant proteins generated showed no major structural or ligand-binding differences compared with the wild-type IFABP (Tables 1 and 2). The structural stability of the mutant proteins was not unexpected, since point mutations of other members of the FABP family have also been shown to be remarkably stable (12, 14), and the covalent incorporation of several fluorescein moieties into the IFABP structure did not alter its folding and ligand binding properties (41). The absence of effects on the ligand binding site was also expected, since IFABP lysines are all oriented toward the aqueous milieu (22) and do not interact with the ligand located in the binding pocket. Instead, they are accessible for interaction with the polar head groups of acceptor membrane phospholipids.

Charge neutralization of three of the four Lys residues of the α-helical domain (K16I, K20I, and K27I) decreases the FA transfer rate to zwitterionic vesicles, compared with the wild-type protein. K29I, in contrast, shows a behavior indistinguishable from the wild type protein. Neutralization of lysine 27 (K27I) results in the most dramatic effect, decreasing the absolute transfer rate and markedly diminishing the sensitivity to SUV concentration. Modifications in the two Lys residues of the α_1 helix induce very similar changes in the FA transfer kinetics. Neutralization of residues 16 and 20 decreases the ligand transfer rate to EPC-SUVs; however, the charge reversal mutants were less affected. It is possible that maintaining the polar face of the α_1 amphipathic helix results in a kinetic behavior similar to the wild type, whereas a disruption of the α_1 amphipathicity, caused by the incorporation of Ile, disrupts the putative protein-membrane interactions.

The dramatic increase in AOFA transfer rate from wild-type IFABP to negatively charged CL vesicles was blunted 2–4-fold for the α_1 helix mutants, indicating that loss of each of the positively charged residues diminished somewhat the protein's sensitivity to acceptor charge. Thus, unlike FA transfer to zwitterionic acceptor membranes, maintaining the α_1 helix amphipathicity by retaining a charged residue of either sign has the same effect on transfer to acidic vesicles as did the disruption of the amphipathicity by replacement of a charged residue with an uncharged residue. This suggests the importance of the interactions of cationic residues with anionic phospholipids. For the α_2-helix, such charge-

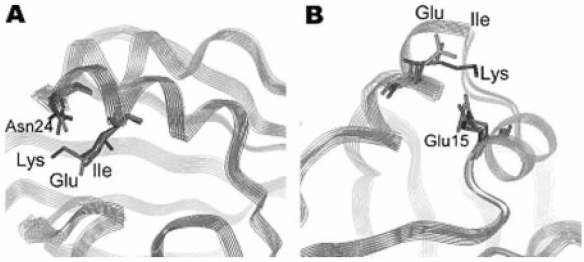

FIGURE 6. **Superimposition of rat intestinal FABP and α_2 Lys mutant structures after energy minimization based on the IFABP-palmitate complex x-ray crystal structure (19) (Protein Data Bank code 2IFB).** The protein molecule is oriented to show the different orientation of residues in the α_2 helix most clearly. *A*, residues 24 and 27 have been *highlighted* to show the altered interaction caused by the K27I and K27E mutations over the putative ligand portal domain. *B*, residues 15 and 29 have been *highlighted* to show the likely disruption of the stabilizing salt bridge between them caused by the K29I and K29E mutations.

charge interactions appear even more essential for FA transfer properties. For both K27E and K29E, sensitivity to acceptor vesicle charge is almost completely abolished relative to wild-type IFABP, probably demonstrating electrostatic repulsion between the Glu residues and the acidic groups in the membrane. In contrast, replacement of the basic residues Lys^{27} and Lys^{29} with isoleucine resulted in less than a 2-fold decrement in the proteins' sensitivity to acceptor negative charge. This systematic and significant difference observed for charge reversal compared with neutralization highlights the importance of charge-charge interaction of the α_2 helix with membranes and suggests that the charged face of the α_2 helix is critical for membrane interactions that lead to the dramatic increase in AOFA transfer rates from IFABP to anionic membranes.

The higher AOFA transfer rates obtained for the neutralization mutants compared with the reversion mutants could also be a consequence of a contribution of Ile in positions 27 and 29 to the hydrophobic patch observed in the IFABP tertiary structure; the α_2 hydrophobic residues Val^{25}, Val^{26}, and Leu^{30} point away from the interior of the protein, forming the only hydrophobic patch on the protein surface (21). We have recently shown that both electrostatic and hydrophobic interactions contribute to the collision-mediated FA transfer mechanism for IFABP (16). Thus, an increase in the hydrophobic character of the α_2 helix could offset to some extent the loss of the electrostatic interactions of Lys^{27} and Lys^{29} with acidic membranes.

The α_2 helix is a key structural element of the putative fatty acid portal, and forms long range interactions with the β_2 turn between strands C and D. The present studies indicate that it is likely to play a role in the fatty acid transfer process as well. NMR solution structures of the apo and holo forms of IFABP have demonstrated considerably greater differences from those initially suggested by crystallographic analysis (7). Notably, the distal half of the α_2 helix and the turn between β-strands C and D are the regions of the protein that exhibit the largest structural differences; both of these portal domain elements were found to be more disordered in the absence of bound ligand and to exhibit diminished long range interactions (7). This suggests that during ligand exit/entry, a conformational change may take place in this region of the protein, allowing the fatty acid to pass through the portal. In addition, mutations in the α_2 helix and C-D turn of heart FABP and adipocyte FABP were shown to alter the rate of AOFA transfer to membranes, further indicating the participation of α_2 in collisional transfer of fatty acids (12, 13). For IFABP, mutations at lysine 27 show the largest changes in response to both acceptor vesicle concentration and charge. Neutralization of lysine 27 markedly diminishes the sensitivity to SUV concentration but maintains sensitivity to SUV charge, whereas substitution for glutamic acid at position 27 eliminates the sensitivity to charge but maintains some sensitivity to SUV concentration, which is probably secondary to diminished protein-membrane interactions. In the holoprotein, Lys^{27} is oriented across the portal, forming an interaction with Asn^{24}, which is located at the end of the turn between the two helices. In the apoprotein, by contrast, Lys^{27} points toward the exterior of the molecule (21, 22). Substitution of this lysine is likely to modify the interaction with Asn^{24} and/or with the polar head groups of the phospholipids, thereby contributing to the changes in FA transfer rate observed in the present experiments (Fig. 6*A*).

Lysine 29 is located in one of the most dynamic regions of backbone mobility (7). As for Lys^{27}, neutralization of the residue reduced IFABP sensitivity to acceptor membrane negative charge; charge reversal resulted in a drastic (>85%) loss in sensitivity to CL-containing vesicles. Thus, disruption of the basic character of the α_2 helix disrupts the effective interaction of holo-IFABP with membranes. In contrast to the large differences in AOFA transfer rates from Lys^{29} IFABP mutants to acidic vesicles, mutations in the Lys^{29} position did not produce significant changes in transfer rates to zwitterionic vesicles. It is possible that this unique behavior may be explained by the existence of side chain interactions. Unlike the other lysines examined, in the native protein, lysine 29 forms a surface salt bridge with glutamate 15 on the α_1 helix, a highly conserved residue in the superfamily of cytosolic lipid-binding proteins (21). The salt bridge may help to hold the two helices together, thereby maintaining the stability of the helical cap. The role of surface salt bridges in local and overall protein stability has been described in other proteins (42, 43). A helical cap that lacks the Lys^{29}-Glu^{15} salt bridge, caused by neutralization or reversal of the positive charge, results in an altered behavior compared with the rest of the mutants of the α-helical domain, which can be attributed both to the destabilization of the α-helical domain and to the liberation of the Glu^{15} charge to the aqueous medium. This suggestion is supported by energy minimization of the K29I and K29E mutant structures, as shown in Fig. 6*B*.

In contrast to the α-helix domain lysine mutants, little effect was found following modifications of Lys^{92}, present in β-strand G, with the K92I showing AOFA transfer rates identical to those of the wild-type IFABP for all conditions examined and K92E substitution resulting in a stimulation of AOFA transfer rate identical to that of wild-type IFABP upon CL incorporation into acceptor membranes. K92E substitution did result in an increase in absolute AOFA transfer rates to zwitterionic membranes, however, suggesting that whereas Lys^{92} is not an essential element of the collisional transfer process, the introduction of a negative charge at this position generates the possibility of an additional interaction of this group with the positive charge of the phosphatidylcholine head group on the zwitterionic vesicle.

Physical interaction between the IFABP forms and membranes was directly investigated by analyzing the radioactive labeling of the protein after incubation with a photoactivable reagent, followed by cross-linking photoactivation. Membrane insertion of several proteins has been identified using these reagents (36, 44, 48). The results showed that native IFABP interacted with membranes in an acceptor vesicle charge- and ligand-dependent manner. The dependence on the membrane charge is coincident with our transfer experiments, where the AOFA transfer rate is increased to acceptor membranes containing negatively charged phospholipids. Since the net surface charge of all cytosol-facing membranes is believed to be negative, it seems likely that charge-charge interactions are the primary driving force for IFABP-mediated FA transfer within the cell. It is interesting to note that CL is a relevant constituent of the inner and outer mitochondrial membranes (49), and its involvement in protein-membrane interactions is well appreciated (50). It is possible that the apparently strong interaction and rapid FA transfer rates from IFABP to CL-containing membranes could be sug-

gesting one aspect of its function in FA trafficking to specific metabolic pathways. Indeed, the cross-linking results indicate that IFABP interacts more strongly with membranes to deliver FA to zwitterionic and PS-containing membranes than to extract FA but interacts strongly with CL-containing membranes to facilitate FA transfer in both directions. As expected (8–10), the helixless IFABP showed a markedly diminished degree of membrane interaction compared with wtIFABP. In contrast, cross-linking analysis of the Lys point mutants showed that the interaction of IFABP with membranes is not affected by individual amino acid substitutions. These results are not unexpected, since a cooperative effect of the lysines appears to be responsible for effective interaction with membranes to take place and since no single point mutation completely abolished the effect of acceptor membrane properties on AOFA transfer. It is also important to note that this method may not be sensitive enough to detect small changes in the degree of IFABP-membrane interaction.

The interaction of IFABP with membranes appears to be greater for the holoprotein than the apoprotein. This suggests the formation of different IFABP-membrane collisional complexes for the holo- *versus* apo-IFABP, and is likely reflecting, in part, the conformational differences demonstrated for apo- and holo-IFABP by solution structures (7, 51).

Previously, we suggested (8, 12, 14) that the collision-based transfer of fatty acids from the FABP binding site to model membranes may occur in a multistage process, as follows: stage 1, interaction of FABP with the acceptor membrane; stage 2, conformational transition of the dynamic portal region from the ordered closed state to a more disordered open state; stage 3, dissociation of FA from the ligand binding cavity; and stage 4, association of the FA with the acceptor membrane. For wild-type IFABP, stage 1 would be rate-limiting, and the transfer process exhibits collisional kinetics. For the helixless protein (9), we hypothesized that step 3 was rate-limiting due to complete elimination of steps 1 and 2. Based on the present results, we hypothesize that a stable α_1 helix is necessary for step 1 to occur and that the α_2 helix is of critical importance for steps 1 and 2. Modification of either lysine in α_1 resulted in a decreased rate of transport that was probably caused by decreases in helix stability, decreased interaction with the membrane, or both. For mutant K27I in α_2, it appears that step 1 is markedly dampened, probably reflecting a weak protein-membrane interaction when the acceptor membranes are net neutral. When membranes are negatively charged, the K27I and K29I mutants in α_2 each demonstrated a 50% decrease in sensitivity to this charge, suggesting that the remaining basic residue maintained its charge-charge interactions with the acidic acceptors. In contrast, the α_2 charge reversal mutants K27E and K29E showed a drastic decrease in sensitivity to membrane charge, probably reflecting repulsive effects with negative charges on the membrane that diminished the strength of the protein-membrane interaction, step 1. Given that the side chain of lysine 27 extends over the portal region and that the side chain of lysine 29 stabilizes helix 2-helix 1 interactions, it is likely that step 2 could be modified when either of these Lys are substituted with Ile, resulting in a change in the protein-membrane complex and/or decrease in the rate of the conformational transition of the dynamic portal, thereby causing slower delivery of FA to membranes. The present results also suggest that the collisional complex formed in step 1 and the conformational transition of step 2 may be different, depending on the acceptor vesicle composition. In all experiments to date, however, the transfer data are well fit by a single exponential function, implying that in the case of the Lys point mutants, the rate-limiting step is likely to reflect step 1, a specific protein-membrane interaction. Thus, we hypothesize that the lysine mutations modify the conformation of the IFABP-membrane "collisional complex," resulting in altered fatty acid transfer rates. Although there are no tertiary structures yet available for an FABP-membrane complex, evidence for conformational changes with membrane binding has been obtained using infrared reflection-absorption spectroscopy, where we showed that the secondary structure of wtIFABP in lipid monolayers differed from its solution structure (10). Changes in IFABP structure upon ligand binding, greatest in the ligand portal region, are also supportive of a conformational change (7, 51). Finally, we have shown that fluorescent fatty acid transfer from membrane donors to IFABP occurs via membrane-protein interaction; however, modulation of the transfer rate by membrane and solution properties was different than for transfer from protein to membrane, implying that the collisional complexes for holo-IFABP and apo-IFABP are different (40).

In summary, the present results provide support for the multistep process of FA transfer from IFABP to membranes and support the hypothesis of Hodsdon and Cistola (7) regarding the existence of a portal domain that undergoes conformational changes during FA release. Our results suggest that IFABP interactions with vesicles induce this conformational change and further indicate the possibility of different conformational changes when the protein is delivering ligand to or extracting ligand from membranes of different composition.

Acknowledgments—We are grateful to Dr. R. C. Rossi for providing equipment for specific kinetic measurements, and we gratefully acknowledge G. Franchini for assistance with the CD measurements. The assistance of Rob Muldowney in the molecular modeling is also gratefully acknowledged.

REFERENCES

1. Glatz, J. F. C., and van der Vusse, G. J. (1996) *Prog. Lipid Res.* **35,** 243–282
2. Bass, N. M. (1985) *Chem. Phys. Lipids* **38,** 95–114
3. Hsu, K. T., and Storch, J. (1996) *J. Biol. Chem.* **271,** 13317–13323
4. Córsico, B., Liou, H. L., and Storch, J. (2004) *Biochemistry,* **43,** 3600–3607
5. Kim, H. K., and Storch, J. (1992) *J. Biol. Chem.* **267,** 77–82
6. Storch, J., and Thumser, E. A. (2000) *Biochim. Biophys. Acta* **1486,** 28–44
7. Hodsdon, M. E., and Cistola, D. P. (1997) *Biochemistry* **36,** 1450–1460
8. Córsico, B., Cistola, D. P., Frieden, C., and Storch, J. (1998) *Proc. Natl. Acad. Sci. U. S. A.* **95,** 12174–12178
9. Kim, K., Cistola, D. P., and Frieden, C. (1996) *Biochemistry* **35,** 7553–7558
10. Wu, F., Córsico, B., Flach, C. R., Cistola, D., Storch, J., and Mendelsohn, R. (2001) *Biochemistry* **40,** 1976–1983
11. Herr, F. M., Matarese, V., Bernlohr, D. A., and Storch, J. (1995) *Biochemistry* **34,** 11840–11845
12. Herr, F. M., Aronson, J., and Storch, J. (1996) *Biochemistry* **35,** 1296–1303
13. Liou, H. L., and Storch, J. (2001) *Biochemistry* **40,** 6475–6485
14. Liou, H. L., Kahn, P. C., and Storch, J. (2002) *J. Biol. Chem.* **277,** 1806–1815
15. Thumser, A. E., Tsai, J., and Storch, J. (2001) *J. Mol. Neurosci.* **16,** 143–150
16. Córsico, B., Franchini, G. R., Hsu, K. T., and Storch, J. (2005) *J. Lipid Res.* **46,** 1765–1772
17. LiCata, V. J., and Bernlohr, D. A. (1998) *Proteins Struct. Funct. Genet.* **33,** 577–589
18. Di Pietro, S. M., Córsico, B., Perduca, M., Monaco, H. L., and Santomé, J. A. (2003) *Biochemistry* **42,** 8192–8203
19. Anantharamaiah, G. M., Jones, M. K., and Segrest, J. P. (1993) in *The Amphipathic Helix* (Epand, R. M., ed) pp. 110–143, CRC Press, Inc., Boca Raton, FL
20. Higuchi, R., Krummel, B., and Saiki, R. K. (1988) *Nucleic Acids Res.* **16,** 7351–7667
21. Scapin, G., Gordon, J. I., and Sacchettini, J. C. (1992) *J. Biol. Chem.* **267,** 4253–4269
22. Sacchettini, J. C., Scapin, G., Gopaul, D., and Gordon, J. I. (1992) *J. Biol. Chem.* **267,** 23534–23545
23. Lee, B., and Richards, F. M. (1971) *J. Mol. Biol.* **55,** 379–400
24. Richards, F. M. (1985) *Methods Enzymol.* **115,** 440–469
25. Kajander, T., Kahn, P. C., Passila, S. H., Cohen, D. C., Lehtio, L., Adolfsen, W., Warwicker, J., Schell, U., and Goldman, A. (2000) *Struct. Fold Des.* **8,** 1203–1214
26. Richards, F. M. (1974) *Biophys. Bioeng.* **82,** 1–14
27. Richards, F. M. (1971) *J. Mol. Biol.* **6,** 151–176
28. Storch, J., Bass, N. M., and Kleinfeld, A. M. (1989) *J. Biol. Chem.* **264,** 8708–8713
29. Richieri, G. V., Ogata, R. T., and Kleinfeld, A. M. (1994) *J. Biol. Chem.* **269,** 23918–23930
30. Massey, J. B., Bick, D. H., and Pownall, H. J. (1997) *Biophys. J.* **72,** 1732–1743
31. Storch, J. (1990) *Hepathology* **12,** 1447–1449

32. Roseman, M. A., and Thompson, T. E. (1980) *Biochemistry* **19,** 439–444
33. Huang, C., and Thompson, T. E. (1974) *Methods Enzymol.* **32,** 485–489
34. Storch, J., and Kleinfeld, A. M. (1986) *Biochemistry* **25,** 1717–1726
35. Weber, T., and Brunner, J. (1995) *J. Am. Chem. Soc.* **117,** 3084–3095
36. Córsico, B., Toledo, J. D., and Garda, H. A. (2001) *J. Biol. Chem.* **276,** 16978–16985
37. Laemmli, U. K. (1970) *Nature* **227,** 680–685
38. Clérico, E. M., Peisajovich, S. G., Ceolín, M., Ghiringhelli, P. D., and Ermácora, M. R. (2000) *Biochim. Biophys. Acta* **1476,** 203–218
39. Wootan, M. G., Bass, N. M., Bernlohr, D. A., and Storch, J. (1990) *Biochemistry* **29,** 9305–9311
40. Thumser, E. A., and Storch, J. (2000) *J. Lipid Res.* **41,** 647–656
41. Frieden, C., Jiang, N., Cistola, D. P. (1995) *Biochemistry* **34,** 2724–2730
42. Hennig, M., Darimont, B., Sterner, R., Kirschner, K., and Jansonius, J. N. (1995) *Structure* **3,** 1295–1306
43. Yip, K. S., Stillman, T. J., Britton, K. L., Artymiuk, P. J., Baker, P. J., Sedelnikova, S. E., Engel, P. C., Pasquo, A., Chiaraluce, R., and Consalvi, V. (1995) *Structure* **3,** 1147–1158
44. Weber, T., Paesold, G., Galli, C., Mischler, R., Semenza, G., and Brunner, J. (1994) *J. Biol. Chem.* **269,** 18353–18358
45. Durrer, P., Gaudin, Y., Ruigrok, R. W. H., Graf, R., and Brunner, J. (1995) *J. Biol. Chem.* **270,** 17575–17581
46. Durrer, P., Galli, C., Hoenke, S., Corti, C., Gluck, R., Vorherr, T., and Brunner, J. (1996) *J. Biol. Chem.* **271,** 13417–13421
47. Vergeres, G., Manenti, S., Weber, T., and Sturzinger, C. (1995) *J. Biol. Chem.* **270,** 19879–19887
48. Garner, J., Durrer, P., Kitchen, J., Brunner, J., and Crooke, E. (1998) *J. Biol. Chem.* **273,** 5167–5173
49. Hovius, R., Lambrechts, H., Nicolay, K., and de Kruijff, B. (1990) *Biochim. Biophys. Acta* **1021,** 217–226
50. Schlattner, U., Gehring, F., Vernoux, N., Tokarska-Schlattner, M., Neumann, D., Marcillat, O., Vial, C., and Wallimann, T. (2004) *J. Biol. Chem.* **279,** 24334–24342
51. Hodsdon, M. E., and Cistola, D. P. (1997) *Biochemistry* **25,** 2278–2290

Protein-Membrane Interaction and Fatty Acid Transfer from Intestinal Fatty Acid-binding Protein to Membranes: SUPPORT FOR A MULTISTEP PROCESS

Lisandro J. Falomir-Lockhart, Lisandro Laborde, Peter C. Kahn, Judith Storch and Betina Córsico

J. Biol. Chem. 2006, 281:13979-13989.
doi: 10.1074/jbc.M511943200 originally published online March 21, 2006
